

Galerkin Reduced Order Models for Compressible Flow with Structural Interaction

Matthew F. Barone*, Daniel J. Segalman†, Heidi Thornquist‡
Sandia National Laboratories
Albuquerque, NM 87185

Irina Kalashnikova §
Sandia National Laboratories and Stanford University
Stanford, CA 94305

The Galerkin projection procedure for construction of reduced order models of compressible flow is examined as an alternative discretization of the governing differential equations. The numerical stability of Galerkin models is shown to depend on the choice of inner product for the projection. For the linearized Euler equations, a symmetry transform leads to a stable formulation for the inner product. Boundary conditions for compressible flow that preserve stability of the reduced order model are constructed. Coupling with a linearized structural dynamics model is made possible through the solid wall boundary condition. Preservation of stability for the discrete implementation of the Galerkin projection is made possible using piecewise-smooth finite element bases. Stability of the coupled fluid/structure system is examined for the case of uniform flow past a thin plate. Stability of the reduced order model for the fluid is demonstrated on several model problems, where a suitable approximation basis is generated using proper orthogonal decomposition of a transient computational fluid dynamics simulation.

I. Introduction

Simulation of time-varying, three-dimensional fluid flow remains, and will continue to remain for some time, an expensive endeavor. This reality has motivated efforts to seek reduced order models (ROMs) that capture the essential dynamics of the full simulations, but at a much lower computational cost. Many ROM techniques in fluid mechanics are derived from the Proper Orthogonal Decomposition (POD)/Galerkin projection approach.¹⁻³ The original intent of this approach was to develop low-dimensional models, containing only a

*Aerosciences Dept., MS 0825, mbarone@sandia.gov. Senior Member, AIAA.

†Strategic Initiatives Dept., MS 0557

‡Electrical and Microsystem Modeling Dept., MS 0316

§PhD Candidate, Institute for Computational and Mathematical Engineering, Sandia student intern

few degrees of freedom, to enable and enhance understanding of the nonlinear dynamics of turbulent flows. Since then, other approaches to building ROMs have been proposed, each with its own inherent strengths, including the reduced basis method,⁴ balanced truncation,^{5,6} and goal-oriented ROMs.⁷ The potential usefulness of ROMs has also since expanded to include predictive applications; for example, ROMs have been used in flow controller design,⁸ shape optimization,⁹ and aeroelastic stability analysis.^{10,11}

The use of POD/Galerkin ROMs in a predictive setting raises some fundamental questions. In this setting the ROM may be viewed as an alternative discretization of the governing partial differential equations. As such, the essential properties of any such discretization are stability, consistency, and convergence. In many situations satisfaction of the first two properties guarantees convergence. General results for any of the three properties are lacking for POD/Galerkin models of compressible fluid flow. This leads to practical limitations; for example, a ROM might be stable for a given number modes but unstable for other choices of basis size (see an example of this for a POD model in Bui-Thanh *et al.*⁷).

The present work primarily addresses numerical stability of linear ROMs for compressible flow. The questions of consistency and convergence are not addressed. Generally speaking, a ROM will be consistent with the simulation data used to generate it. The POD basis is not usually complete, which complicates a general consistency analysis. Also not addressed is the related question of the behavior of a ROM when applied to a parameter space region not included in the ROM construction. There are promising developments in this area which can be applied; see, for example, Lieu and Farhat.¹² Despite the lack of a comprehensive theory, it is still desirable to be able to generate a stable ROM regardless of the quality of the POD basis used to generate it. This is analagous to being able to run computational fluid dynamics simulations on a series of meshes, from coarse to fine, and having confidence that the simulations will remain stable regardless of the mesh spacing.

In this work we analyze the POD/Galerkin method as a particular type of spectral approximation method. It is demonstrated that the inner product used to define the Galerkin projection is intimately tied to stability of the resulting model. An energy stability analysis is carried out for Galerkin methods applied to the linearized Euler equations, resulting in an inner product that guarantees certain stability bounds satisfied by the ROM. A means of implementing boundary conditions for the ROM that preserve stability is also developed. Implementation of the ROM is then defined in terms of finite element representations of the simulation data and of the POD modes. Along with numerical quadrature rules of sufficient accuracy, this approach ensures that the continuous stability estimates are satisfied by the discrete computer implementation. A scheme for coupling the linearized Euler equation ROM with a structural dynamics ROM is then developed, and the stability properties of the resulting aeroelastic ROM are examined. ROMs are then constructed for several model fluid flows using the schemes developed from the stability analysis.

II. The POD/Galerkin Approach

This section describes the POD/Galerkin method for reducing the order of computational models for solving partial differential equations. The approach consists of two steps: calculation of a basis using the POD of an ensemble of flowfield realizations, followed by

Galerkin projection of the governing partial differential equations onto the basis. The first step involves the transfer of kinematic information from the high-fidelity simulation to a relatively small number of modes. The second step involves a translation of the full-system dynamics to the implied dynamics of these modes. When successful, the result of this procedure is a set of time-dependent ordinary differential equations in the modal amplitudes that accurately describes the flow dynamics of the full system of PDEs for some limited set of flow conditions.

A. Proper Orthogonal Decomposition

The Proper Orthogonal Decomposition (POD) is a mathematical procedure that, given an ensemble of data, constructs a basis for the ensemble that is optimal in a well-defined sense. The mathematical development of POD for fluid flow applications in particular is described in some detail in Lumley¹³ and Holmes *et al.*³ The essentials of this development and the properties of POD most important to reduced order modeling are presented in this section.

Consider an ensemble $\{\mathbf{u}^k(\mathbf{x})\}$ of real vector fields on the domain $\mathbf{x} \in \Omega$. In the present context, the ensemble consists of a set of instantaneous snapshots of a numerical simulation solution field. The \mathbf{u} 's are assumed to belong to an infinite-dimensional Hilbert space $H(\Omega)$ with associated inner product (\mathbf{f}, \mathbf{g}) . Following the approach of Rowley *et al.*,¹⁴ we will defer the definition of the inner product until a particular application of the POD is considered, requiring only that it obey the usual requirements for an inner product. Note that this results in a general formulation for the POD that differs in some aspects from formulas derived for the $L^2(\Omega)$ Hilbert space.

The POD basis is a set of functions $\{\phi_j(\mathbf{x})\}$ that is the “best” linear basis for description of the ensemble. Since the basis is linear, a flowfield $\mathbf{u} \in \text{span}\{\phi_j\}$ can be represented as a linear combination of the POD modes,

$$\mathbf{u}(\mathbf{x}, t) = \sum_j a_j(t) \phi_j(\mathbf{x}). \quad (1)$$

The POD modes, or empirical eigenfunctions, are defined by requiring that the averaged projection of the ensemble \mathbf{u}^k onto ϕ is a maximum:

$$\max_{\phi \in H(\Omega)} \frac{\langle (\mathbf{u}, \phi)^2 \rangle}{\|\phi\|^2}, \quad (2)$$

where $\|\cdot\|$ is the norm generated by the inner product. The averaging operator $\langle \cdot \rangle$ used in (2) could be an ensemble average over many separate flow realizations, or it could be a time-average taken from different samples of a single realization.

The constrained optimization problem (2) with constraint $\|\phi\| = 1$ reduces to the eigenvalue problem

$$\mathbf{R}\phi = \lambda\phi, \quad (3)$$

where

$$\mathbf{R}\phi \equiv \langle \mathbf{u}^k(\mathbf{u}^k, \phi) \rangle. \quad (4)$$

The operator \mathbf{R} is self-adjoint and non-negative definite; if we further assume that \mathbf{R} is compact, then there exists a countable set of non-negative eigenvalues λ_i , with associated eigenfunctions ϕ_i . The eigenfunctions, appropriately normalized, form an orthonormal subspace of H , i.e. $(\phi_i, \phi_j) = \delta_{ij}$.

The POD modes are the eigenfunctions ϕ_i associated with nonzero λ_i . Taking the inner product of (3) with ϕ , it is straightforward to show that $\langle (\mathbf{u}^k, \phi_i)^2 \rangle = \lambda_i$. In other words, the magnitude of the eigenvalue is equivalent to the average energy of the projection of the ensemble onto the associated eigenfunction, where the square of the inner product is interpreted as an energy measure. The POD modes may be ordered according to the magnitude of their eigenvalue, with λ_1, ϕ_1 equal to the eigenvalue/eigenfunction pair with the largest eigenvalue, λ_N equal to the smallest non-zero eigenvalue, and $\lambda_1 > \lambda_2 > \dots > \lambda_n > \dots > \lambda_N$. In building reduced order models one is interested in truncating the POD basis and retaining only the $M < N$ most energetic modes. It can be shown that the sequence of truncated POD bases forms an optimal set, in the sense that a POD basis comprised of M modes describes more energy (on average) of the ensemble than any other *linear* basis of the same dimension M . This compression of the ensemble energy into a minimum number of modes makes the POD basis attractive for reduced order modeling.

In practice, the \mathbf{u}^k are vectors of state variables at discrete grid point locations, each containing a single solution from the numerical simulation. They will have length Nr , where N is the total number of grid points and r is the number of dependent variables describing the flow state. Thus, the discretized version of (3) will be an eigenvalue problem of order Nr . For $N \gg K$, where K is the number of flowfield snapshots used, this procedure is costly and, it turns out, inefficient. Sirovich¹⁵ showed how the eigenvalue problem (3) can be reduced to order K , resulting in a much more efficient procedure for $N \gg K$. This is the so-called ‘‘method of snapshots’’ for computing a POD basis.

B. Galerkin Projection

The second step for constructing the reduced order model is to project the governing PDEs onto the POD basis.

Consider a generic nonlinear PDE, containing a linear term as well as quadratic and cubic nonlinearities, that governs the behavior of a time-dependent vector field $\mathbf{u}(\mathbf{x}, t)$,

$$\frac{\partial \mathbf{u}}{\partial t} = \mathcal{L}\mathbf{u} + \mathcal{N}_2(\mathbf{u}, \mathbf{u}) + \mathcal{N}_3(\mathbf{u}, \mathbf{u}, \mathbf{u}). \quad (5)$$

The operator \mathcal{L} is a linear operator, \mathcal{N}_2 is a quadratic nonlinear operator, and \mathcal{N}_3 is a cubic nonlinear operator. The Galerkin projection of equation (5) onto each POD mode ϕ_j is

$$\left(\frac{\partial \mathbf{u}}{\partial t}, \phi_j \right) = (\mathcal{L}\mathbf{u}, \phi_j) + (\mathcal{N}_2(\mathbf{u}, \mathbf{u}), \phi_j) + (\mathcal{N}_3(\mathbf{u}, \mathbf{u}, \mathbf{u}), \phi_j). \quad (6)$$

Substituting the POD decomposition for \mathbf{u} into (6), applying the algebraic rules of inner products along with orthogonality of the POD basis gives

$$\frac{da_k}{dt} = \sum_l a_l (\phi_k, \mathcal{L}(\phi_l)) + \sum_{l,m} a_l a_m (\phi_k, \mathcal{N}_2(\phi_l, \phi_m)) + \sum_{l,m,n} a_l a_m a_n (\phi_k, \mathcal{N}_3(\phi_l, \phi_m, \phi_n)). \quad (7)$$

This is the reduced order model for equation (5) by the POD/Galerkin method. It is a time-dependent system of ODE's of order equal to the number of retained POD modes M , with $k = 1, 2, \dots, M$. The inner products in (7) are functionals of the known, time-independent POD modes $\phi(\mathbf{x})$, and may be precomputed before integration of the ROM.

The Galerkin projection step here is applied to the original, continuous PDEs. In many applications of reduced order modelling, the discrete representation of the equations is projected onto the modes. This discrete approach has the advantage that, depending on the implementation, boundary condition terms present in the discretized equation set are inherited by the ROM. Also, certain properties of the numerical scheme used to solve the full equations may be inherited by the ROM. The continuous approach, used in the present work, has the advantages that it does not require an intrusive or code-specific implementation and it may be more amenable to analysis.

C. Inner Product

The inner product serves several purposes in the POD/Galerkin procedure. Fundamentally, it helps define the Hilbert space on which the analysis proceeds. It defines the projection of a solution onto the POD basis, and thereby also defines the mathematical quantity that the POD basis optimally represents. It also defines the projection of the governing equations onto the POD basis, which leads to the POD/Galerkin dynamical model.

The majority of POD/Galerkin models for fluid flow have used the incompressible Navier-Stokes equations as the governing equation set. In this case, a natural choice of inner product is the L^2 inner product, defined here on the spatial domain Ω ,

$$(u, v) = \int_{\Omega} u v \, d\Omega. \quad (8)$$

This is because if the solution vector is taken to be the velocity vector u_i , then the inner product corresponds to a measure of the global kinetic energy. This makes the POD basis physically sensible, since the modes optimally represent the kinetic energy present in the ensemble from which they are generated. This choice also leads to a straightforward representation of the solution energy in terms of modal amplitudes. If the POD representation of the solution is

$$u_i = \sum_{k=1}^M a_k(t) \phi_i^k(\mathbf{x}), \quad (9)$$

then the global kinetic energy at any instant in time is

$$2E = (u_i, u_i) = \sum_{k=1}^M a_k^2. \quad (10)$$

III. Stability of Galerkin approximations

This section examines stability of Galerkin approximations to a class of linear partial differential equations, as well as stability of such approximations to equations governing linearized compressible flow. In the initial theoretical development, C^∞ smooth solutions

and equation coefficients are assumed. The smoothness assumption will be relaxed when the discrete computer implementation of the method is discussed.

A. Stability for Linear Equations

Consider the initial-value problem, or Cauchy problem,

$$\frac{\partial u}{\partial t} = Lu, \quad x \in \mathbf{R}^n, \quad t \geq 0, \quad (11)$$

$$u(x, 0) = f(x). \quad (12)$$

Here L is a linear differential operator with constant coefficients. The operator L is *semi-bounded* w.r.t. the inner product $(\cdot, \cdot)_E$ if it satisfies the following inequality for all sufficiently smooth functions $w = w(x)$, $w \in L^2$,

$$(w, Lw)_E \leq \alpha(w, w)_E, \quad (13)$$

where α is a real constant. In this case well-posedness follows from the relation

$$\frac{d}{dt}(u, u)_E \leq \alpha(u, u)_E. \quad (14)$$

In fact, the following theorem holds:¹⁶

The Cauchy problem given by (11) is well-posed if and only if the operator L is semi-bounded w.r.t. an inner product $(\cdot, \cdot)_E$ which corresponds to a norm equivalent to the L_2 -norm.

Now consider a Galerkin approximation to (11), $u_N \in \mathcal{H}$, satisfying

$$\left(\frac{\partial u_N}{\partial t}, \phi \right)_E = (Lu_N, \phi)_E \quad (15)$$

for all $\phi \in \mathcal{H}$, and suppose that L is semi-bounded w.r.t. $(\cdot, \cdot)_E$. Setting $\phi = u_N$ leads to the following stability estimate for the Galerkin approximation.^{17,18}

$$\frac{1}{2} \frac{d}{dt} \|u_N\|_E^2 \leq \alpha \|u_N\|_E^2 \quad (16)$$

Thus,

$$\|u_N(x, t)\|_E \leq e^{\alpha t} \|u_N(x, 0)\|_E. \quad (17)$$

The result (17) means that the numerical solution is bounded in a way consistent with behavior of exact solutions of the original differential equation, *i.e.* it is stable. The practical implication of these results is the opportunity to pose a stable Galerkin approximation to a well-posed linear differential equation by choosing an appropriate inner product, one with respect to which the differential operator is semi-bounded. These results can be extended to variable-coefficient operators, including linear hyperbolic systems of equations such as the linearized Euler equations (discussed in the next section).

B. Stability of the Galerkin approximation for compressible flow

1. Stability for a Linear Hyperbolic System of Equations

This section presents the energy method analysis of Gustafsson and Sundstrom.¹⁹ First consider a linear hyperbolic system of equations for $x \in R^n$

$$\frac{\partial u}{\partial t} + A_j \frac{\partial u}{\partial x_j} + Cu = 0 \quad (18)$$

where A_j and C are smooth functions of space but do not vary with time. Suppose that this equation can be symmetrized by introduction of a positive definite symmetric matrix H ,

$$H \frac{\partial u}{\partial t} + HA_j \frac{\partial u}{\partial x_j} + HCu = 0 \quad (19)$$

such that HA_j are each symmetric matrices. Then, using the symmetry properties of H and HA_j , the following energy expression is derived:

$$\begin{aligned} \frac{\partial}{\partial t} \int_{\Omega} u^T H u \, d\Omega = \\ - \int_{\partial\Omega} u^T H (A_j n_j) u \, dS + \int_{\Omega} u^T \left(\frac{\partial}{\partial x_j} (HA_j) - HC - C^T H \right) u \, d\Omega \end{aligned} \quad (20)$$

Now consider the pure initial value problem, ignoring the contribution from the boundary surface integral in (20). Noting that H can be decomposed into $H = Q^T Q$, the right hand side of (20) is

$$\begin{aligned} \int_{\Omega} u^T \left(\frac{\partial}{\partial x_j} (HA_j) + HC + C^T H \right) u \, d\Omega = \\ \int_{\Omega} u^T Q^T \left(Q^{T-1} \frac{\partial}{\partial x_j} (HA_j) Q^{-1} - Q C Q^{-1} - (Q C Q^{-1})^T \right) Q u \, d\Omega. \end{aligned} \quad (21)$$

Thus (20) becomes

$$\frac{\partial}{\partial t} \int_{\Omega} u^T H u \, d\Omega \leq 2\alpha \int_{\Omega} u^T H u \, d\Omega, \quad (22)$$

where 2α is an upper bound on the eigenvalues of

$$Q^{T-1} \frac{\partial}{\partial x_j} (HA_j) Q^{-1} - Q C Q^{-1} - (Q C Q^{-1})^T.$$

The integral $(u, v)_H \equiv \int_{\Omega} u^T H v \, d\Omega$ is an energy inner product. The corresponding energy norm $\|u\|_H = (u, u)_H^{1/2}$ is equivalent to the L^2 norm and establishes well-posedness (recall section III.A) by satisfying

$$\|u(x, t)\|_H \leq e^{\alpha t} \|u(x, 0)\|_H. \quad (23)$$

In turn, the corresponding Galerkin approximation u_N using the energy norm satisfies the stability condition

$$\|u_N(x, t)\|_H \leq e^{\alpha t} \|u_N(x, 0)\|_H. \quad (24)$$

2. Stability for the Linearized Euler Equations

If a compressible fluid system can be described by inviscid, small-amplitude perturbations about a steady-state mean flow, then the linearized Euler equations may be used. In the following development, stability estimates for the linearized Euler equation initial value problem are derived, which lead to stability of Galerkin approximations using appropriate inner products. The stability results follow from the results of the previous section, since the linearized Euler equations are a symmetrizable hyperbolic system of PDEs.

Let the fluid state vector be decomposed into a steady mean and time-varying fluctuating part, $\mathbf{q}(\mathbf{x}, t) = \bar{\mathbf{q}}(\mathbf{x}) + \mathbf{q}'(\mathbf{x}, t)$, where $\mathbf{q} = [u \ v \ w \ \zeta \ p]^T$. The three components of the velocity vector are u , v , and w , the specific volume is ζ , and the pressure is p . The density ρ is the inverse of the specific volume. The linearized Euler equations in these variables are:

$$\frac{\partial \mathbf{q}'}{\partial t} + \mathbf{A}(\bar{\mathbf{q}}) \cdot \nabla \mathbf{q}' + C(\bar{\mathbf{q}}) \mathbf{q}' = 0 \quad (25)$$

where

$$\mathbf{A}(\bar{\mathbf{q}}) \equiv [A_x(\bar{\mathbf{q}}), A_y(\bar{\mathbf{q}}), A_z(\bar{\mathbf{q}})]^T,$$

$$A_x = \begin{bmatrix} \bar{u} & 0 & 0 & 0 & \bar{\zeta} \\ 0 & \bar{u} & 0 & 0 & 0 \\ 0 & 0 & \bar{u} & 0 & 0 \\ -\bar{\zeta} & 0 & 0 & \bar{u} & 0 \\ \gamma \bar{p} & 0 & 0 & 0 & \bar{u} \end{bmatrix} \quad A_y = \begin{bmatrix} \bar{v} & 0 & 0 & 0 & 0 \\ 0 & \bar{v} & 0 & 0 & \bar{\zeta} \\ 0 & 0 & \bar{v} & 0 & 0 \\ 0 & -\bar{\zeta} & 0 & \bar{v} & 0 \\ 0 & \gamma \bar{p} & 0 & 0 & \bar{v} \end{bmatrix} \quad A_z = \begin{bmatrix} \bar{w} & 0 & 0 & 0 & 0 \\ 0 & \bar{w} & 0 & 0 & 0 \\ 0 & 0 & \bar{w} & 0 & \bar{\zeta} \\ 0 & 0 & -\bar{\zeta} & \bar{w} & 0 \\ 0 & 0 & \gamma \bar{p} & 0 & \bar{w} \end{bmatrix}$$

$$C = \begin{bmatrix} \frac{\partial \bar{u}}{\partial x} & \frac{\partial \bar{u}}{\partial y} & \frac{\partial \bar{u}}{\partial z} & \frac{\partial \bar{p}}{\partial x} & 0 \\ \frac{\partial \bar{v}}{\partial x} & \frac{\partial \bar{v}}{\partial y} & \frac{\partial \bar{v}}{\partial z} & \frac{\partial \bar{p}}{\partial y} & 0 \\ \frac{\partial \bar{w}}{\partial x} & \frac{\partial \bar{w}}{\partial y} & \frac{\partial \bar{w}}{\partial z} & \frac{\partial \bar{p}}{\partial z} & 0 \\ \frac{\partial \bar{\zeta}}{\partial x} & \frac{\partial \bar{\zeta}}{\partial y} & \frac{\partial \bar{\zeta}}{\partial z} & -\left(\frac{\partial \bar{u}}{\partial x} + \frac{\partial \bar{v}}{\partial y} + \frac{\partial \bar{w}}{\partial z}\right) & 0 \\ \frac{\partial \bar{p}}{\partial x} & \frac{\partial \bar{p}}{\partial y} & \frac{\partial \bar{p}}{\partial z} & 0 & \gamma \left(\frac{\partial \bar{u}}{\partial x} + \frac{\partial \bar{v}}{\partial y} + \frac{\partial \bar{w}}{\partial z}\right) \end{bmatrix}$$

In this case the symmetrizing matrix H is given by

$$H = \begin{bmatrix} \bar{\rho} & 0 & 0 & 0 & 0 \\ 0 & \bar{\rho} & 0 & 0 & 0 \\ 0 & 0 & \bar{\rho} & 0 & 0 \\ 0 & 0 & 0 & \alpha^2 \gamma \bar{\rho}^2 \bar{p} & \bar{\rho} \alpha^2 \\ 0 & 0 & 0 & \bar{\rho} \alpha^2 & \frac{(1+\alpha^2)}{\gamma \bar{p}} \end{bmatrix} \quad (26)$$

where α^2 is an arbitrary real, nonzero parameter. The ‘‘symmetry inner product’’ is then ^a

$$(\mathbf{q}'^{(1)}, \mathbf{q}'^{(2)})_H = \int_{\Omega} \left[\bar{\rho} \left(u'^{(1)} u'^{(2)} + v'^{(1)} v'^{(2)} + w'^{(1)} w'^{(2)} \right) + \alpha^2 \gamma \bar{\rho}^2 \bar{p} \zeta'^{(1)} \zeta'^{(2)} + \frac{1 + \alpha^2}{\gamma \bar{p}} p'^{(1)} p'^{(2)} + \alpha^2 \bar{\rho} \left(\zeta'^{(2)} p'^{(1)} + \zeta'^{(1)} p'^{(2)} \right) \right] d\Omega. \quad (27)$$

Due to the result for linear hyperbolic systems given by equation (24), Galerkin approximations for the linearized Euler equations based on the inner product $(\cdot, \cdot)_H$ are stable (for the initial value problem). Introducing a modal basis $\mathbf{q}' = \sum_{k=1}^M a_k(t) \phi_k(\mathbf{x})$ with

$$\phi_j = \left[\phi_j^1 \quad \phi_j^2 \quad \phi_j^3 \quad \phi_j^4 \quad \phi_j^5 \right]^T, \quad (28)$$

the Galerkin projection is

$$\left(\phi_j, \frac{\partial \mathbf{q}'}{\partial t} \right)_H + (\phi_j, \mathbf{A}(\bar{\mathbf{q}}) \cdot \nabla \mathbf{q}')_H + (\phi_j, C(\bar{\mathbf{q}}) \mathbf{q}')_H = 0. \quad (29)$$

Substituting the modal basis into (29) leads to the ROM,

$$\dot{a}_j = - \sum_{k=1}^M a_k (\phi_j, \mathbf{A}(\bar{\mathbf{q}}) \cdot \nabla \phi_k)_H - \sum_{k=1}^M a_k (\phi_j, C(\bar{\mathbf{q}}) \phi_k)_H. \quad (30)$$

Note that for a spatially uniform mean state, the right-hand side of (20) is zero, $\|\mathbf{q}'\|_H$ is conserved, and the semi-discrete Galerkin approximation satisfies the strong stability condition

$$\|\mathbf{q}'(t)\|_H \leq \|\mathbf{q}'(0)\|_H. \quad (31)$$

The uniform mean flow case allows for a clean stability analysis, since the mean flow supports only neutral or decaying disturbances. For non-uniform flow the continuous equations may support exponentially growing instabilities, an example of which is the Kelvin-Helmholtz shear layer instability. It is then difficult to distinguish between natural instability modes supported by the continuous equations and spurious instabilities generated by the numerical discretization.

Note that the symmetry inner product introduced here is only directly applicable to Galerkin approximations of the *linearized* Euler equations. One could consider adapting this inner product to a Galerkin treatment of the full nonlinear Euler equations by specifying a steady mean flow and projecting the resulting quasi-linear equations using the symmetry inner product. This would not necessarily lead to a stable approximation, since the fluctuations about the specified mean state will, in general, be nonlinear. However, in practice this may provide a superior inner product than other naïve choices, *e.g.* the L^2 inner product.

^aThis form of the symmetrization follows the derivation of Gustafsson and Sundstrom.¹⁹ Other symmetric forms of both the linearized Euler and linearized Navier-Stokes equations can be found in Olinger and Sundstrom²⁰ and in Abarbanel and Gottlieb.²¹ In an earlier work, Chu²² derived a disturbance energy equation using a similar inner product without explicit consideration of symmetrization.

This situation differs from the usual stability arguments applied to finite difference/finite volume type discretizations of hyperbolic equations. There, the stability of the discretization for linearized “frozen coefficient” equations leads to stability of the method when applied to the corresponding nonlinear equations. This is due to the fact that implementation of these methods uses the same type of time-linearization as that of the stability analysis. For a POD/Galerkin method of the type considered here, this is not possible since both the POD computation and the projection depend upon a specified weighted inner product, the weights of which are not a function of time.

IV. Fluid ROM Boundary Conditions

Boundary conditions may be efficiently implemented for a Galerkin ROM using a weak formulation. Further, the energy stability analysis of section III.B allows for weak boundary conditions that preserve stability.

Consider Galerkin projection of the linearized Euler equations onto a modal basis $\{\phi_j\}$. Integrating the second term of (29) by parts gives

$$\begin{aligned} (\phi_j, \mathbf{A}(\bar{\mathbf{q}}) \cdot \nabla \mathbf{q}')_H &= \int_{\partial\Omega} \phi_j^T H(\bar{\mathbf{q}}) (\mathbf{A}(\bar{\mathbf{q}}) \cdot \mathbf{n}) \mathbf{q}' \, dS \\ &\quad - \int_{\Omega} (\nabla \cdot [\phi_j^T H(\bar{\mathbf{q}}) \mathbf{A}(\bar{\mathbf{q}})]) \mathbf{q}' \, d\Omega. \end{aligned} \quad (32)$$

Boundary conditions may now be implemented through modification of the perturbed state in the surface integral appearing in (32). Implementation is simplified if the ROM without boundary conditions is calculated first, according to (30). Denoting the unmodified boundary integral $I_{bu_{jk}} \equiv \int_{\partial\Omega} \phi_j^T H(\bar{\mathbf{q}}) (\mathbf{A}(\bar{\mathbf{q}}) \cdot \mathbf{n}) \phi_k \, dS$ and the boundary integral with boundary conditions enforced as $I_{b_{jk}}$, the ROM becomes

$$\dot{a}_j = - \sum_{k=1}^M a_k (\phi_j, \mathbf{A}(\bar{\mathbf{q}}) \cdot \nabla \phi_k)_H - \sum_{k=1}^M a_k (\phi_j, C(\bar{\mathbf{q}}) \phi_k)_H + \sum_{k=1}^M a_k (I_{bu_{jk}} - I_{b_{jk}}). \quad (33)$$

The effect of a particular boundary condition on stability is easily investigated by examining the sign on the boundary integral term. A ROM that is stable for the initial value problem will remain stable if $\int_{\partial\Omega} \phi_j^T H(\bar{\mathbf{q}}) (\mathbf{A}(\bar{\mathbf{q}}) \cdot \mathbf{n}) \mathbf{q}' \, dS \geq 0$.

A. Solid Surface Boundary Condition

The linearized no-penetration boundary condition for a surface with unit normal \mathbf{n} (pointing out of the fluid domain), displaced a small distance η from equilibrium, and moving at velocity $\dot{\eta}$ in the direction of $-\mathbf{n}$, is

$$\mathbf{u}' \cdot \mathbf{n} = -\dot{\eta} - \bar{\mathbf{u}} \cdot \nabla \eta \equiv u'_b. \quad (34)$$

Assuming that the base flow satisfies $\bar{\mathbf{u}} \cdot \mathbf{n} = 0$, the product $(\mathbf{A}(\bar{\mathbf{q}}) \cdot \mathbf{n}) \mathbf{q}'$ is

$$(\mathbf{A}(\bar{\mathbf{q}}) \cdot \mathbf{n}) \mathbf{q}' = \begin{pmatrix} n_1 \bar{\zeta} p' \\ n_2 \bar{\zeta} p' \\ n_3 \bar{\zeta} p' \\ -\bar{\zeta} \mathbf{u}' \cdot \mathbf{n} \\ \gamma \bar{p} \mathbf{u}' \cdot \mathbf{n} \end{pmatrix} \quad (35)$$

Applying the boundary condition (34) to (35) and multiplying by $\phi_j^T H(\bar{\mathbf{q}})$ gives the required surface integrand:

$$\phi_j^T H(\bar{\mathbf{q}}) (\mathbf{A}(\bar{\mathbf{q}}) \cdot \mathbf{n}) \mathbf{q}' = (n_1 \phi_j^1 + n_2 \phi_j^2 + n_3 \phi_j^3) p' + \phi_j^5 u'_b. \quad (36)$$

Note that if the POD modes are obtained from simulations with a stationary surface then, at least within the accuracy of the no-penetration boundary condition enforcement in the simulations, $n_1 \phi_j^1 + n_2 \phi_j^2 + n_3 \phi_j^3 = 0$. In the absence of a moving surface in the ROM, $u'_b = 0$ as well, and no boundary condition integral is required. Thus, the stability results of section III.B for the initial value problem are unaltered.

Inserting the modal representation for p' into (36), and applying the surface integral over the no-penetration surface $\partial\Omega_P$, leads to the following term appearing in the ROM:

$$\begin{aligned} I_{P_{jk}} &= \int_{\partial\Omega_P} \phi_j^T H(\bar{\mathbf{q}}) (\mathbf{A}(\bar{\mathbf{q}}) \cdot \mathbf{n}) \phi_k \, dS \\ &= \sum_{k=1}^M a_k(t) \int_{\partial\Omega_P} (n_1 \phi_j^1 + n_2 \phi_j^2 + n_3 \phi_j^3) \phi_k^5 \, dS + \int_{\partial\Omega_P} \phi_j^5 u'_b \, dS. \end{aligned} \quad (37)$$

The second term in (37) is a forcing term due to the nonhomogenous wall velocity. The effect of the first term on stability is not immediately clear; its impact on ROM stability will need to be assessed in *a posteriori* tests after the ROM has been constructed.

B. Far-field Boundary Condition

Far-field conditions may be useful and, in some cases, necessary for stability of a ROM formulation. Presumably the CFD code used to generate the fluid modal basis incorporates some form of farfield boundary condition which, if it is a linear boundary condition, will also be satisfied by the fluid modes due to the properties of POD. However, to ensure a well-posed and stable Galerkin approximation, farfield boundary conditions can be incorporated into the ROM. Consider the boundary integral term from (32) evaluated over a farfield boundary $\partial\Omega_F$. Application of an approximately non-reflecting far-field boundary condition is accomplished using a locally one-dimensional characteristic formulation. The matrix $\mathbf{A}(\bar{\mathbf{q}}) \cdot \mathbf{n}$ may be diagonalized using the transformation

$$\mathbf{A}(\bar{\mathbf{q}}) \cdot \mathbf{n} = S \Lambda S^{-1}, \quad (38)$$

where the vector of ‘‘characteristic variables’’ is defined as

$$\mathbf{V}' = S^{-1} \mathbf{q}' \quad (39)$$

The far-field boundary integral may then be cast as:

$$\begin{aligned}
I_F &= \int_{\partial\Omega_F} \phi_j^T H(\bar{\mathbf{q}}) [\mathbf{A}(\bar{\mathbf{q}}) \cdot \mathbf{n}] \mathbf{q}' dS \\
&= \int_{\partial\Omega_F} \phi_j^T H(\bar{\mathbf{q}}) S \Lambda S^{-1} \mathbf{q}' dS \\
&= \int_{\partial\Omega_F} \phi_j^T [H(\bar{\mathbf{q}}) S \Lambda] \mathbf{V}' dS
\end{aligned} \tag{40}$$

The procedure for application of an approximately non-reflecting condition is as follows. The components of \mathbf{V}' corresponding to characteristic waves traveling into the domain are set to zero. The terms in the boundary integrand are re-cast in terms of the modal representation, which leads to boundary terms in the ROM. It can be proved that this boundary condition formulation results in $I_F \geq 0$, which, along with the stability analysis of section III.B, guarantees stability of the initial-boundary value problem. The details of the far-field boundary condition implementation are given in the Appendix.

V. Approximation Space and Numerical Quadrature

Thus far, the stability estimates and associated inner products for Galerkin ROMs have only been given in continuous form. They are valid only if the relevant integrals are evaluated exactly. This is similar to the situation occurring in numerical analysis of spectral methods. With spectral methods, this problem is generally resolved by applying a high-precision numerical quadrature that is able to exactly integrate the spectral projections. We borrow from this approach in the following way. The POD basis is first described by a finite element representation on the computational mesh. This is fairly general, as long as the simulation code can output data to a nodal mesh, and the mesh can be cast as a collection of finite elements. In the present work we use piecewise-linear (C^0) finite elements to represent the snapshot data and the POD modes. It is then possible to construct a numerical quadrature operator that exactly integrates the inner product of the finite element representations. The introduction of C^0 finite elements requires a relaxation of the smoothness requirements on \mathbf{q}' , $H(\bar{\mathbf{q}})$, and $\mathbf{A}(\bar{\mathbf{q}})$. The projection integrals are then to be interpreted in the sense of distributions.

Consider the d -dimensional spatial domain Ω , subdivided into N_e elements, $\Omega_e, e = 1, \dots, N_e$. The finite element representation of the state variable \mathbf{q}' is

$$\mathbf{q}'^h(\mathbf{x}) = \sum_{i=1}^{N_n} N_i(\mathbf{x}) \mathbf{q}'_i, \quad \mathbf{x} \in \Omega_e \tag{41}$$

where N_n is the number of nodes that define the element Ω_e , and N_i are the linear shape functions. Consider the case of linear tetrahedral elements, where $N_n = 4$ and the shape functions span the space of all possible linear functions on the element. A quadratic function $f(\mathbf{x})$ can be integrated exactly over an element by a quadratic Gauss quadrature rule of the form

$$\int_{\Omega} f(\mathbf{x}) d\Omega_e = \sum_{j=1}^4 \omega'_{j_e} f(\mathbf{x}_{j_e}), \tag{42}$$

where ω'_{j_e} are the integration weights and the \mathbf{x}_{j_e} are the Gauss integration points of the element.

Now suppose the integral to be computed is a weighted inner product of two state vector realizations $\mathbf{u}(\mathbf{x})$ and $\mathbf{v}(\mathbf{x})$,

$$(\mathbf{u}, \mathbf{v})_H = \int_{\Omega} \mathbf{u}^T H(\bar{\mathbf{q}}) \mathbf{v} \, d\Omega. \quad (43)$$

The discrete representations of the vectors \mathbf{u} and \mathbf{v} are written as \mathbf{u}^h and \mathbf{v}^h , respectively, with length equal to the number of mesh nodes N times the dimension of the vector, r . Let $H_e^h(\bar{\mathbf{q}})$ be the $r \times r$ element inner product matrix, taken to be piecewise constant over each element. The formula for numerical integration can be written

$$(\mathbf{u}, \mathbf{v})_H = \mathbf{u}^{hT} W \mathbf{v}^h \quad (44)$$

where W is a sparse block matrix comprised of $N \times N$ blocks of dimension $r \times r$. The k - l th block of W is $w_{kl} I$, with

$$w_{kl} = \sum_{e=1}^{N_{kl}^e} H_e^h \sum_{j=1}^4 N_{ke}(\mathbf{x}_{j_e}) N_{le}(\mathbf{x}_{j_e}) \omega'_{j_e}, \quad (45)$$

and where the outer sum is over the elements connected to the k - l nodal ‘‘edge.’’

The finite element representation and associated Gauss quadratures allow for a general and flexible means of creating stable, projection-based ROMs. The only requirements are that data is stored at nodes of the mesh and that the mesh can be decomposed into finite elements of the desired order. Higher order representations of the base flow and inner product matrix $H(\bar{\mathbf{q}})$ are also possible, given a quadrature rule of sufficient order.

VI. Coupled Fluid/Structure ROM

Construction of a coupled fluid/structure ROM proceeds using a segregated approach, where separate fluid and structural ROMs are built and then combined together to form the coupled ROM. We consider as a first case the linear structural vibration of a thin plate surrounded on one side by a uniform compressible fluid, with velocity vector $(\bar{u}, 0, 0)$. The plate is square with length L , density ρ_s , bending stiffness D_{bend} , thickness h , and positioned in the $z = 0$ plane. The PDE governing the (small) transverse deflection field $\eta(x, y, t)$ in the presence of an unsteady pressure loading $p(x, y, z, t)$ is

$$\rho_s h \frac{\partial^2 \eta}{\partial t^2} + D_{bend} \nabla^4 \eta = -p'(x, y, 0, t). \quad (46)$$

In this simple model problem, the structural ROM is just a Galerkin approximation using several plate eigenmodes. The solution for η is expanded as

$$\eta(x, y, t) = \sum_{k=1}^P b_k(t) \xi_k(x, y). \quad (47)$$

This leads to the following set of modal structural equations

$$(\rho_s h) \ddot{b}_k + \left(D_{bend} \int_{\partial\Omega_P} \nabla^4 \xi_k \xi_k \, dS \right) b_k = - \int_{\partial\Omega_P} \xi_k p'(x, y, 0, t) \, dS, \quad k = 1, \dots, P \quad (48)$$

where $(u, v)_{L_2}^P \equiv \int_{\partial\Omega_P} u v \, dS$.

The coupling matrices are

$$B = \left(\begin{array}{ccc|ccc} (\phi_1^5, \bar{u} \frac{\partial \xi_1}{\partial x})_{L_2}^P & \cdots & (\phi_1^5, \bar{u} \frac{\partial \xi_P}{\partial x})_{L_2}^P & (\phi_1^5, \xi_1)_{L_2}^P & \cdots & (\phi_1^5, \xi_P)_{L_2}^P \\ \vdots & & \vdots & \vdots & & \vdots \\ \vdots & \ddots & \vdots & \vdots & \ddots & \vdots \\ \vdots & & \vdots & \vdots & & \vdots \\ (\phi_M^5, \bar{u} \frac{\partial \xi_M}{\partial x})_{L_2}^P & \cdots & (\phi_M^5, \bar{u} \frac{\partial \xi_P}{\partial x})_{L_2}^P & (\phi_M^5, \xi_1)_{L_2}^P & \cdots & (\phi_M^5, \xi_P)_{L_2}^P \end{array} \right) \quad (55)$$

$$\equiv \left(\tilde{B}_{M \times P} \mid \tilde{C}_{P \times M}^T \right)$$

$$C = \left(\begin{array}{ccc} 0_{P \times M} \\ \hline -\frac{1}{\rho_s h} (\phi_1^5, \xi_1)_{L_2}^P & \cdots & -\frac{1}{\rho_s h} (\phi_M^5, \xi_1)_{L_2}^P \\ \vdots & \ddots & \vdots \\ -\frac{1}{\rho_s h} (\phi_1^5, \xi_P)_{L_2}^P & \cdots & -\frac{1}{\rho_s h} (\phi_M^5, \xi_P)_{L_2}^P \end{array} \right) \equiv \left(\begin{array}{c} 0_{P \times M} \\ \hline \frac{-1}{\rho_s h} \tilde{C}_{P \times M} \end{array} \right) \quad (56)$$

A. Stability of the Coupled System

1. Useful Prior Results

In analyzing the stability of the coupled system (50), we will make use of the following theorems, proven in Ref. 23. First, a definition, quoted from Ref. 23:

Definition 3.1 from Ref. 23. We say that [the matrix] K is ‘stable’ if and only if:

1. K is diagonalizable in \mathbb{C} .
2. $\forall \lambda \in Sp(K), \mathcal{R}(\lambda) \leq 0$.

Theorem 3.1 from Ref. 23. A real, symmetric positive definite (RSPD) matrix E_K is an energy matrix for K if and only if for all X that solve $\dot{X} = KX$, $\frac{1}{2} \frac{d}{dt} (X^T E_K X) \leq 0$.

Theorem 3.4 from Ref. 23. If A and D are two real, stable matrices with energy matrices E_A and E_D , then

$$\{E_A B + (E_D C)^T = 0\} \Rightarrow \left\{ K = \begin{pmatrix} A & B \\ C & D \end{pmatrix} \text{ is a stable matrix.} \right\} \quad (57)$$

2. Energy Matrices

The energy matrices for the fluid and structure systems assume a relatively simple form. It is easily verified that $E_A = I$ is an energy matrix for A when $\nabla\bar{q} = 0$. This follows from

$$\frac{1}{2} (F^T E_A F) = \frac{1}{2} (F^T F) = \frac{1}{2} \sum_{k=1}^M a_k^2(t) = \frac{1}{2} (\mathbf{q}', \mathbf{q}')_H \quad (58)$$

The analysis of section III.B shows that $\frac{1}{2} \frac{d}{dt} (F^T E_A F) \leq 0$, assuming stable application of boundary conditions.

Turning now to the structure, the matrix

$$E_D = \left(\begin{array}{c|c} \tilde{L}_{P \times P} & 0_{P \times P} \\ \hline 0_{P \times P} & (\rho_s h) I_{P \times P} \end{array} \right) \quad (59)$$

is an energy matrix for D . Carrying out the algebra,

$$S^T E_D D S = -\dot{\mathbf{b}}(t)^T \tilde{L}_{P \times P} \mathbf{b}(t) + \mathbf{b}(t)^T \tilde{L}_{P \times P} \dot{\mathbf{b}}(t) = 0 \quad (60)$$

It follows from (60) that $\frac{1}{2} \frac{d}{dt} (S^T E_D S) = 0$, meaning E_D defined above is an energy matrix.

3. Stability result

Theorem A.1. Under the uniform base flow assumption ($\nabla\bar{q} \equiv 0$), $K = \begin{pmatrix} A & B \\ C & D \end{pmatrix}$ defining the coupled system is a stable matrix if $\bar{u} = 0$.

Proof. By Theorem 3.4 in Ref. 23, K is a stable matrix if $E_A B + (E_D C)^T = 0$. The matrix sum of interest is

$$\begin{aligned} E_A B + (E_D C)^T &= E_A B + C^T E_D^T \\ &= I \left(\tilde{B}_{M \times P} \mid -\tilde{C}_{P \times M}^T \right) + \left(0_{M \times P} \mid \frac{1}{\rho_s h} \tilde{C}_{P \times M}^T \right) \left(\begin{array}{c|c} \tilde{L}_{P \times P} & 0_{P \times P} \\ \hline 0_{P \times P} & (\rho_s h) I_{P \times P} \end{array} \right) \\ &= \left(\tilde{B}_{M \times P} \mid -\tilde{C}_{P \times M}^T \right) + \left(0_{M \times P} \mid \tilde{C}_{P \times M}^T \right) \\ &= \left(\tilde{B}_{M \times P} \mid 0_{P \times M} \right) \end{aligned} \quad (61)$$

(61) is the zero matrix if $\tilde{B}_{M \times P} = 0$. Clearly this holds if $\bar{u} = 0$, so $\bar{u} = 0 \Rightarrow E_A B + (E_D C)^T = 0$. □

Note that the system *can* be stable for non-zero \bar{u} ; it is just not guaranteed to remain stable. In the case where $\bar{u} = 0$, the structure cannot extract energy from the mean flow, as occurs in flutter. For $\bar{u} \neq 0$, an aero-elastic analysis proceeds by determining the conditions under which the eigenvalues of K will have positive real part. For supersonic flow, it turns out that once \bar{u} exceeds a certain threshold (the flutter speed), the system becomes linearly unstable.

VII. Results

A. ROM generation procedure

For the results presented in this section, the fluid simulation data were generated using the AERO-F simulation code.²⁴ AERO-F is an Arbitrary Lagrangian-Eulerian code that can be used for high-fidelity aeroelastic analysis. The linearized Euler solver capability of AERO-F was used in the present work; details of the finite volume discretization and linearization can be found in Lieu *et al.*¹¹

The fluid POD modes are generated by solution of an eigenproblem, as explained in section II. A code was written that reads in the snapshot data written by AERO-F, assembles the necessary finite element representation of the fields, and computes the numerical quadrature necessary for computation of the inner products. The code performs all the calculations in parallel using distributed matrix and vector data structures and parallel eigensolvers from the Trilinos project,²⁵ allowing for large data sets and a relatively large number of POD modes. The `libmesh` finite element library²⁶ was used to compute element quadratures. This code also projects the modes onto the linearized Euler equations and outputs the resulting fluid ROM coefficient matrix A .

B. Test Case: Random Basis

To demonstrate the stability properties of the fluid ROM, we first consider the case where the modal basis is comprised of a sequence of random vector fields that decay to zero at the boundary. The spatial domain is a rectangular prism, discretized by tetrahedral elements. The base flow is taken to be spatially uniform; such a flow is physically stable to any linear disturbance. Projecting the linearized Euler equations onto the random basis leads to a linear ROM, written here as

$$\dot{a}_j = A_{jk} a_k \quad (62)$$

The ROM is stable if the maximum real part of the eigenvalues of the matrix A_{jk} , denoted $\lambda_{r_{max}}$, is less than zero. Figure 1 plots $\lambda_{r_{max}}$ for ROMs consisting of one through eight basis functions. Using the symmetry inner product $(\cdot, \cdot)_H$ to construct the ROM results in a $\lambda_{r_{max}}$ of zero to machine precision. This is completely consistent with convection of a neutral disturbance in uniform flow, and confirms that for any modal basis, this property of the linearized Euler equations is preserved. For comparison, a second set of ROMs was constructed by nondimensionalizing the modes, and using the unweighted L^2 inner product, equation (8), to project the equations. The nondimensionalization used was $\zeta^* = \zeta/\bar{\zeta}$, $u^* = u/\bar{c}$, $v^* = v/\bar{c}$, $w^* = w/\bar{c}$, $p^* = p/\bar{\rho}\bar{c}^2$, where $*$ quantities are non-dimensional. As seen in the figure, depending on the number of modes used in the ROM, the ROM can be

stable or unstable. While this is a somewhat extreme case using “bad” modes, it is often the case that POD modes with small energy are largely comprised of numerical error and other high-frequency “noise.” The symmetry inner product method ensures that such modes will not destabilize the ROM.

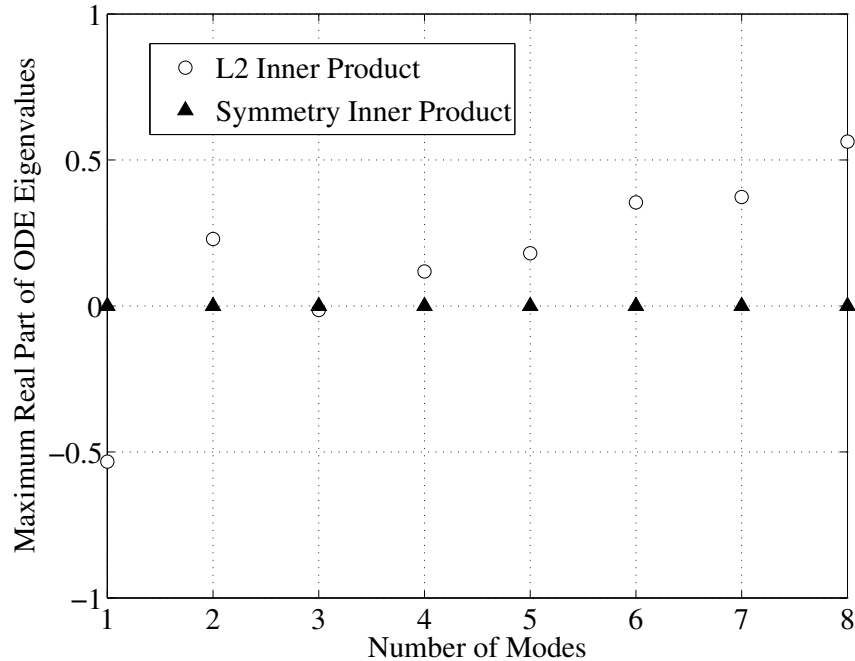


Figure 1. Maximum real part of the eigenvalues of the ROM coefficient matrix A_{jk} for the case of random modes on a uniform base flow.

C. Test Case: Propagation of a One-dimensional Acoustic Pulse

A fluid-only ROM is now constructed using CFD solutions of the following simple model problem. A one-dimensional acoustic pulse is prescribed as the initial condition,

$$u' = \exp(-(x - x_0)^2), \quad p' = \bar{\rho} \bar{c} u', \quad \frac{\rho'}{\bar{\rho}} = \left(\frac{p'}{\bar{p}} \right)^{\frac{1}{\gamma}} \quad v' = w' = 0 \quad (63)$$

The mean flow is taken as a uniform flow at Mach number $M = 0.5$. The pulse convects in the positive x direction at speed $\bar{u} + \bar{c}$, maintaining its shape. This problem was solved on a three-dimensional rectangular prism domain, with extent $0 \leq x \leq 20$, $-5 \leq y \leq 5$, $0 \leq z \leq 1$. The grid was composed of unstructured tetrahedral elements. Slip wall boundary conditions were applied on the constant y and z boundaries. The CFD simulation was performed over a nondimensional time $T_{tot} = 5.25$ with a total of 512 time steps. Snapshots were saved every 8 simulation time steps and used to construct a 16 mode POD basis. Using the symmetry inner product, this basis captured essentially 100 percent of the snapshot energy (to six digits), while 8 modes of this basis captured 99.5 percent and 4 modes 85.5 percent. The L^2 basis was very similar in terms of energy capture of the snapshots.

Four different procedures were used to generate a fluid ROM for this problem: symmetry inner product with and without slip wall boundary conditions, and unweighted L^2 inner product with and without slip wall boundary conditions. The CFD simulations apply the slip wall condition only weakly, so that in general non-zero velocities were generated normal to the slip walls, resulting in non-zero boundary integrals in the ROM construction. Figure 2 shows the maximum real part of the ROM eigenvalues for the different types of ROM. Only the symmetry inner product with boundary conditions leads to a stable ROM. In this case the computed maximum real part of the eigenvalues was less than 10^{-9} . The ROMs without boundary conditions are not stable, regardless of the inner product, and the L^2 ROM with boundary conditions is the most unstable. These results show that the symmetry formulation guarantees ROM stability, but only with the proper boundary conditions enforced. Note that the instabilities in all cases are very weak for this test case; accuracy of the ROMs over the solution time used to generate the ROM is comparable in each case. However, this is a relatively simple flow and stability properties in more complex flows may be less benign. Figure 3 shows the symmetry/with boundary conditions ROM solution for several modes, compared to the projection of the full CFD simulation onto the modes.

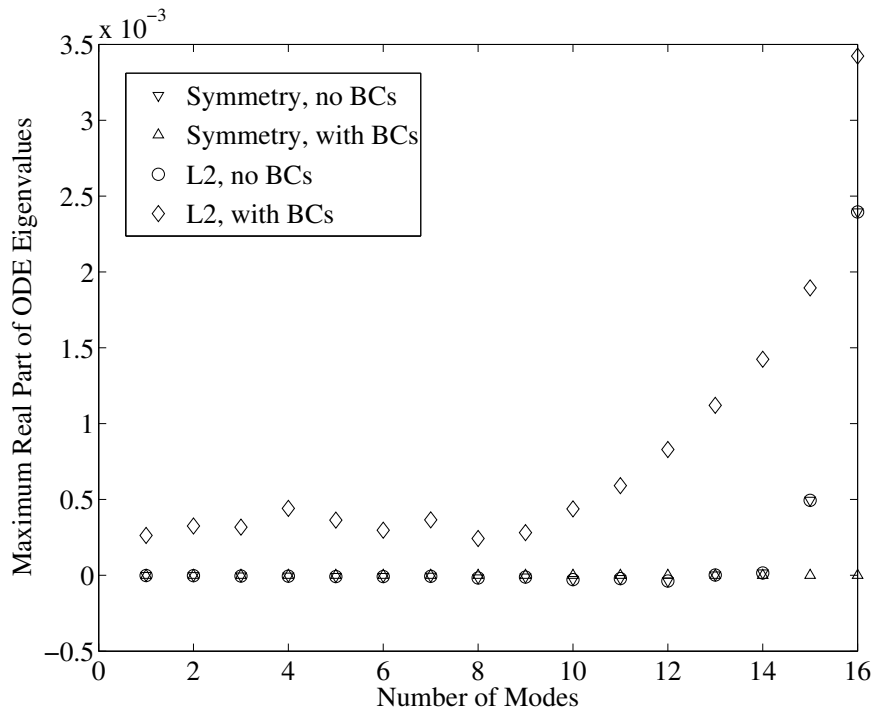


Figure 2. Maximum real part of the eigenvalues of the ROM coefficient matrix A_{jk} for the pulse flow.

D. Test Case: Reflection of a Two-dimensional Pressure Pulse

A slightly more complicated situation is considered in this problem, where a two-dimensional pressure pulse reflects from walls of the domain. The mean flow is taken to be uniform with

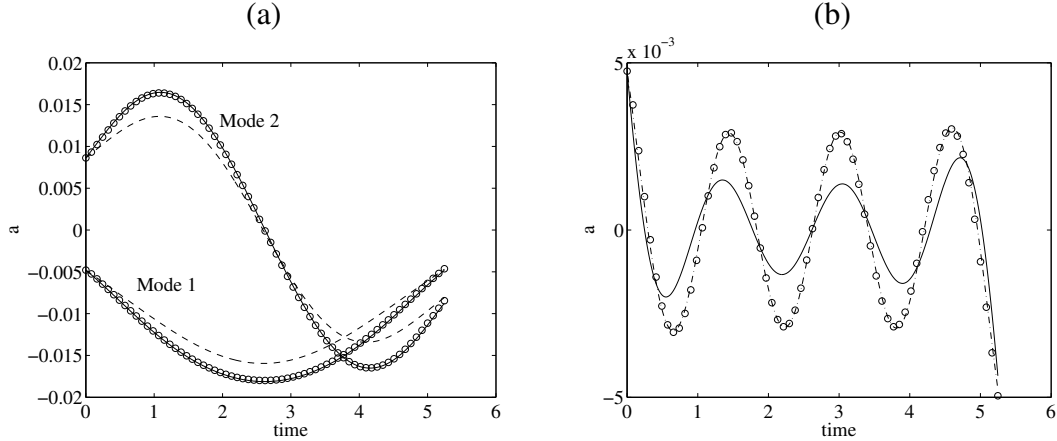


Figure 3. Time history of modal amplitudes for acoustic pulse problem. \circ , CFD simulation. $---$, 4 Mode ROM. $—$, 8 Mode ROM. $- \cdot -$ 12 Mode ROM. (a) Modes 1 and 2. (b) Mode 8.

$M = 0.25$. The initial condition is taken as

$$p' = \exp(-((x - x_0)^2 + (y - y_0)^2)), \quad \frac{\rho'}{\bar{\rho}} = \left(\frac{p'}{\bar{p}}\right)^{\frac{1}{\gamma}}, \quad u' = v' = w' = 0 \quad (64)$$

The same grid used in the previous section for the one-dimensional pulse is used here, with slip wall boundary conditions applied as before. The CFD simulation was run for a non-dimensional time of $T_{tot} = 7.2$ using 704 time steps. Snapshots were saved every 8 time steps beginning with time step number 56, and these were used to generate the POD basis.

The symmetry inner product with boundary conditions applied again produced a stable ROM. Figure 4 compares the projection of the CFD solution onto the first four modes (containing 80 percent of the snapshot energy) with the ROM prediction using 16 modes. Qualitative agreement is good, but with noticeable quantitative errors. Figure 5 compares the CFD pressure disturbance field with the field reconstructed from the ROM solution at $t = 5.0$. The reflection from the upper and lower walls is qualitatively captured by the ROM. The difference between the CFD simulation and the ROM solution could be from two sources. The first possibility is that the POD basis is not rich enough to capture all of the relevant dynamics of the expanding and reflecting pulse. This might be remedied by collecting more snapshots and computing more POD modes. The second possibility is that there is significant error in the CFD solution, which manifests as error (of a different character) in the ROM. Recall that the quality of a ROM solution reflects the quality of the simulation used to generate the basis. We have not yet systematically examined the effects of both of these error sources but plan to do so in future work.

VIII. Conclusions

A method for computing reduced order models for linearized compressible flow has been developed and tested. The primary contribution of this new formulation is the introduction of a symmetry inner product for the linearized Euler equations which is guaranteed to produce stable ROMs. Accompanying boundary conditions have also been developed to

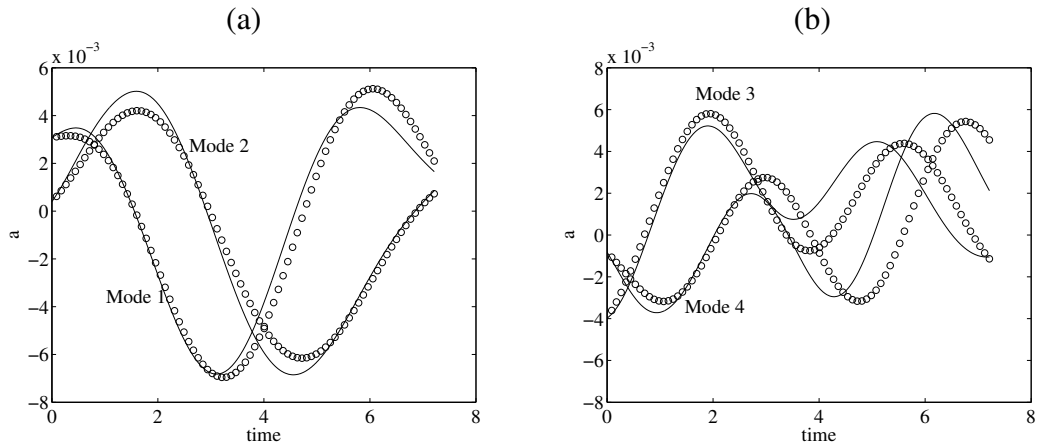


Figure 4. Time history of modal amplitudes for two-dimensional pressure pulse problem. \circ , CFD simulation. —, 16 Mode ROM (a) Modes 1 and 2. (b) Modes 3 and 4.

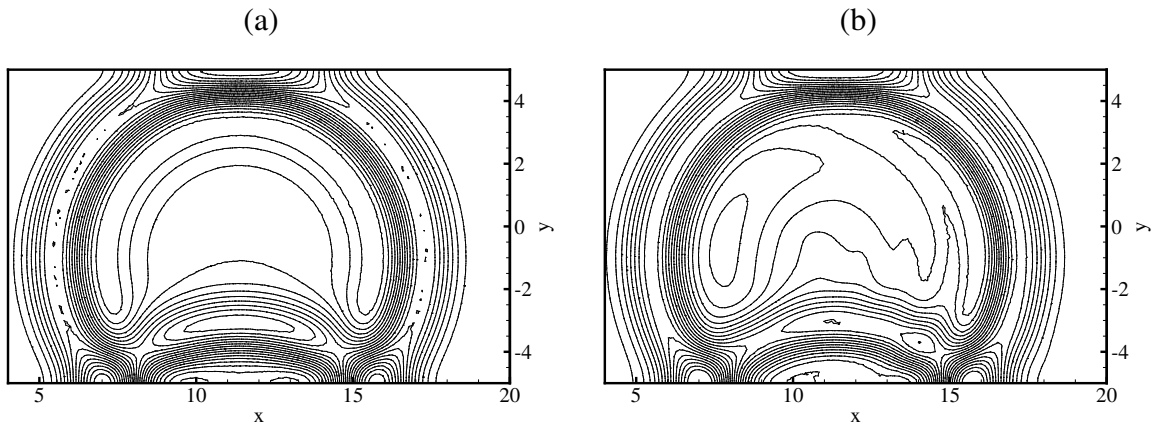


Figure 5. Pressure disturbance contours for the two-dimensional reflected pulse case, $t = 5.0$. (a) CFD result. (b) ROM result.

preserve numerical stability for the case of the bounded domain. A method for coupling the fluid ROM to a structural dynamics ROMs has also been given, but has not yet been tested. These tests will be addressed in future work.

The fluid ROM example problems presented show that the present formulation does indeed produce stable ROMs. However, in these examples the instabilities produced by other inner product choices are only weak instabilities that do not have a practical effect on ROM accuracy. This is not to be expected in every case. For example, consider a time-periodic flow that one wishes to run for very long times. In such a flow, even weak instabilities can result in solution blow-up for long enough simulation times. The value of a stable ROM formulation is clear in such a case.

In future work we will consider application of stable Galerkin ROMs to more complicated flows and geometries, including flows with non-uniform base flow. We also plan to apply some of the mathematical principles used to develop symmetry inner products to the nonlinear Euler equations, in anticipation of an improved method for generating nonlinear ROMs.

IX. Acknowledgements

The authors gratefully acknowledge Thuan Lieu and Charbel Farhat of Stanford University for providing us with the AERO-F code and associated user-support. Sandia is a multiprogram laboratory operated by Sandia Corporation, a Lockheed Martin Company for the United States Department of Energy's National Nuclear Security Administration under contract DE-AC04-94AL85000.

References

- ¹L. Sirovich. Turbulence and the dynamics of coherent structures, Part III: Dynamics and scaling. *Quarterly of Applied Mathematics*, 45(3):583–590, 1987.
- ²N. Aubry, P. Holmes, J. Lumley, and E. Stone. The dynamics of coherent structures in the wall region of a turbulent boundary layer. *J. Fluid Mech.*, 192:115–173, 1988.
- ³P. Holmes, J.L. Lumley, and G. Berkooz. *Turbulence, coherent structures, dynamical systems and symmetry*. Cambridge University Press, 1996.
- ⁴K. Veroy and A.T. Patera. Certified real-time solution of the parametrized steady incompressible Navier-Stokes equations: rigorous reduced-basis *a posteriori* error bounds. *Int. J. Num. Meth. Fluids*, 47:773–788, 2005.
- ⁵K. Willcox and J. Peraire. Balanced model reduction via the proper orthogonal decomposition. *AIAA J.*, 40(11):2323–2330, 2002.
- ⁶C. W. Rowley. Model reduction for fluids, using balanced proper orthogonal decomposition. *Int. J. Bifurcation and Chaos*, 15(3):997–1013, 2005.
- ⁷T. Bui-Thanh, K. Willcox, O. Ghattas, and B. van Bloemen Waanders. Goal-oriented, model-constrained optimization for reduction of large-scale systems. *J. Comp. Phys.*, 224:880–896, 2007.
- ⁸J.A. Taylor and M.N. Glauser. Towards practical flow sensing and control via POD and LSE based low-dimensional tools. *J. Fluids Eng.*, 126(3):337–345, 2003.
- ⁹P. A. LeGresley and J. J. Alonso. Investigation of non-linear projection for POD based reduced order models for aerodynamics. AIAA Paper 2001-0926, 39th AIAA Aerospace Sciences Meeting & Exhibit, 2001.
- ¹⁰K.C. Hall, J.P. Thomas, and E.H. Dowell. Proper orthogonal decomposition technique for transonic unsteady aerodynamic flows. *AIAA J.*, 38(10), 2000.
- ¹¹T. Lieu, C. Farhat, and M. Lesoinne. Reduced-order fluid/structure modeling of a complete aircraft configuration. *Comput. Methods Appl. Mech. Engrg.*, 195:5730–5742, 2006.
- ¹²T. Lieu and C. Farhat. Aerodynamic parameter adaptation of CFD-based reduced-order models. AIAA Paper 2007-328, 45th Aerospace Sciences Meeting and Exhibit, 2007.
- ¹³J.L. Lumley. *Stochastic tools in turbulence*. Academic Press, New York, 1971.
- ¹⁴C.W. Rowley, T. Colonius, and R.M. Murray. Model reduction for compressible flows using POD and Galerkin projection. *Physica D*, 189:115–129, 2004.
- ¹⁵L. Sirovich. Chaotic dynamics of coherent structures. *Physica D*, 37:126–145, 1989.
- ¹⁶H. O. Kreiss and J. Lorenz. *Initial-Boundary Value Problems and the Navier-Stokes Equation*. Academic Press, Inc., 1989.
- ¹⁷D. Gottlieb and S.A. Orszag. *Numerical Analysis of Spectral Methods*. SIAM, 1977.
- ¹⁸W. J. Layton. Stable Galerkin methods for hyperbolic systems. *SIAM J. Numer. Anal.*, 20(2):221–233, 1983.
- ¹⁹B. Gustafsson and A. Sundström. Incompletely parabolic problems in fluid dynamics. *SIAM J. Appl. Math.*, 35(2):343–357, 1978.
- ²⁰J. Oliger and A. Sundström. Theoretical and practical aspects of some initial boundary-value problems in fluid dynamics. *SIAM J. Appl. Math.*, 35(3):419–446, 1978.

²¹S. Abarbanel and D. Gottlieb. Optimal time splitting for two- and three-dimensional Navier-Stokes equations with mixed derivatives. *J. Comp. Phys*, 35:1–33, 1981.

²²B.-T. Chu. On the energy transfer to small disturbances in fluid flow (Part I). *Acta Mechanica*, 1(3):215–234, 1965.

²³S. Piperno, C. Farhat, and B.Larroutoutou. Partitioned procedured for the transient solution of coupled aeroelastic problems. *Comp. Methods Appl. Mech. Engrg.*, 124:79–112, 1995.

²⁴C. Farhat, P. Geuzaine, and G. Brown. Application of a three-field nonlinear fluid-structure formulation to the prediction of the aeroelastic parameters of an F-16 fighter. *Computers & Fluids*, 32:3–29, 2003.

²⁵Michael A. Heroux, Roscoe A. Bartlett, Vicki E. Howle, Robert J. Hoekstra, Jonathan J. Hu, Tamara G. Kolda, Richard B. Lehoucq, Kevin R. Long, Roger P. Pawlowski, Eric T. Phipps, Andrew G. Salinger, Heidi K. Thornquist, Ray S. Tuminaro, James M. Willenbring, Alan Williams, and Kendall S. Stanley. An overview of the trilinos project. *ACM Trans. Math. Softw.*, 31(3), 2005.

²⁶B. Kirk, J. W. Peterson, R. H. Stogner, and G. F. Carey. libMesh: A C++ Library for Parallel Adaptive Mesh Refinement/Coarsening Simulations. *Engineering with Computers*, 22(3–4):237–254, 2006.

X. Appendix: Far-field Boundary Conditions

The matrices that diagonalize $\mathbf{A}(\bar{\mathbf{q}}) \cdot \mathbf{n}$ according to equation (38) are

$$S = \begin{pmatrix} 0 & n_3 & n_2 & \frac{1}{2}n_1 & -\frac{1}{2}n_1 \\ n_3 & 0 & -n_1 & \frac{1}{2}n_2 & -\frac{1}{2}n_2 \\ -n_2 & -n_1 & 0 & \frac{1}{2}n_3 & -\frac{1}{2}n_3 \\ n_1 & -n_2 & n_3 & -\frac{\bar{\zeta}}{2c} & -\frac{\bar{\zeta}}{2c} \\ 0 & 0 & 0 & \frac{\gamma\bar{p}}{2c} & \frac{\gamma\bar{p}}{2c} \end{pmatrix} \quad (65)$$

$$S^{-1} = \begin{pmatrix} 0 & n_3 & -n_2 & n_1 & \frac{\bar{\zeta}n_1}{\gamma\bar{p}} \\ n_3 & 0 & -n_1 & -n_2 & -\frac{\bar{\zeta}n_2}{\gamma\bar{p}} \\ n_2 & -n_1 & 0 & n_3 & \frac{\bar{\zeta}n_3}{\gamma\bar{p}} \\ n_1 & n_2 & n_3 & 0 & \frac{c}{\gamma\bar{p}} \\ -n_1 & -n_2 & -n_3 & 0 & \frac{c}{\gamma\bar{p}} \end{pmatrix} \quad (66)$$

$$\Lambda = \begin{pmatrix} \bar{u}_n & 0 & 0 & 0 & 0 \\ 0 & \bar{u}_n & 0 & 0 & 0 \\ 0 & 0 & \bar{u}_n & 0 & 0 \\ 0 & 0 & 0 & \bar{u}_n + c & 0 \\ 0 & 0 & 0 & 0 & \bar{u}_n - c \end{pmatrix} \quad (67)$$

The vector of characteristic variables is then

$$\mathbf{V}' \equiv S^{-1}\mathbf{q}' = \begin{pmatrix} (n_3v' - n_2w' + n_1\zeta') + \frac{\bar{\zeta}}{\gamma\bar{p}}n_1p' \\ (n_3u' - n_1w' - n_2\zeta') - \frac{\bar{\zeta}}{\gamma\bar{p}}n_2p' \\ (n_2u' - n_1v' + n_3\zeta') + \frac{\bar{\zeta}}{\gamma\bar{p}}n_3p' \\ u'_n + \frac{c}{\gamma\bar{p}}p' \\ -u'_n + \frac{c}{\gamma\bar{p}}p' \end{pmatrix} \quad (68)$$

In terms of the ROM basis $\phi_k(\mathbf{x}) \equiv \left(\phi_k^1(\mathbf{x}) \ \phi_k^2(\mathbf{x}) \ \phi_k^3(\mathbf{x}) \ \phi_k^4(\mathbf{x}) \ \phi_k^5(\mathbf{x}) \right)^T$, $k = 1, \dots, M$, the characteristic variables are

$$V' = \begin{pmatrix} \sum_{k=1}^M \left[n_1 \left(\phi_k^4 + \left(\frac{\bar{\zeta}}{c} \right)^2 \phi_k^5 \right) - n_2 \phi_k^3 + n_3 \phi_k^2 \right] a_k(t) \\ \sum_{k=1}^M \left[-n_1 \phi_k^3 - n_2 \left(\phi_k^4 + \left(\frac{\bar{\zeta}}{c} \right)^2 \phi_k^5 \right) + n_3 \phi_k^1 \right] a_k(t) \\ \sum_{k=1}^M \left[-n_1 \phi_k^2 + n_2 \phi_k^1 + n_3 \left(\phi_k^4 + \left(\frac{\bar{\zeta}}{c} \right)^2 \phi_k^5 \right) \right] a_k(t) \\ \sum_{k=1}^M \left[n_1 \phi_k^1 + n_2 \phi_k^2 + n_3 \phi_k^3 + \frac{\bar{\zeta}}{c} \phi_k^5 \right] a_k(t) \\ \sum_{k=1}^M \left[-n_1 \phi_k^1 - n_2 \phi_k^2 - n_3 \phi_k^3 + \frac{\bar{\zeta}}{c} \phi_k^5 \right] a_k(t) \end{pmatrix} \quad (69)$$

Recall that the farfield boundary integrand from equation (40) is $\phi_j^T [H(\bar{\mathbf{q}})\Lambda] \mathbf{V}'$. The portion $\phi_j^T [H(\bar{\mathbf{q}})\Lambda]$ is given by

$$\phi_j^T [H(\bar{U})S\Lambda] = \begin{pmatrix} [\bar{\rho}n_3\phi_j^2 - \bar{\rho}n_2\phi_j^3 + \alpha^2\bar{\rho}n_1(\gamma\bar{\rho}\bar{p}\phi_j^4 + \phi_j^5)] \bar{u}_n \\ [\bar{\rho}n_3\phi_j^1 - \bar{\rho}n_1\phi_j^3 - \alpha^2\bar{\rho}n_2(\gamma\bar{\rho}\bar{p}\phi_j^4 + \phi_j^5)] \bar{u}_n \\ [\bar{\rho}n_2\phi_j^1 - \bar{\rho}n_1\phi_j^2 + \alpha^2\bar{\rho}n_3(\gamma\bar{\rho}\bar{p}\phi_j^4 + \phi_j^5)] \bar{u}_n \\ \frac{1}{2} [\bar{\rho}n_1\phi_j^1 + \bar{\rho}n_2\phi_j^2 + \bar{\rho}n_3\phi_j^3 + \frac{1}{c}\phi_j^5] (\bar{u}_n + c) \\ \frac{1}{2} [-\bar{\rho}n_1\phi_j^1 - \bar{\rho}n_2\phi_j^2 - \bar{\rho}n_3\phi_j^3 - \frac{1}{c}\phi_j^5] (\bar{u}_n - c) \end{pmatrix}^T \equiv \begin{pmatrix} d_1(\mathbf{x}) \\ d_2(\mathbf{x}) \\ d_3(\mathbf{x}) \\ d_4(\mathbf{x}) \\ d_5(\mathbf{x}) \end{pmatrix}^T \quad (70)$$

The boundary conditions are implemented by altering, as required, the elements of the characteristic variable vector \mathbf{V}' that correspond to incoming characteristics. The present treatment applies an approximately non-reflecting condition, that is the elements of \mathbf{V}' corresponding to incoming characteristics are set to zero. Incoming characteristics are those with negative associated characteristic speed; the characteristic speeds are the diagonal entries of the matrix Λ . There are four possibilities:

1. Case 1: Supersonic Inflow ($\bar{u}_n < -c$)

Note that $\bar{u}_n < -c < 0 \Rightarrow \bar{u}_n - c < 0$ and $\bar{u}_n + c < 0$, i.e., all the characteristics are incoming. The approximate non-reflecting BC mandates that all incoming characteristics be set to zero. The far-field BC is thus

$$V'_b \equiv \mathbf{0} \in \mathbb{R}^5 \quad (71)$$

It follows that I_F in (40) reduces to

$$I_F \equiv 0 \quad (72)$$

2. Case 2: Subsonic Inflow ($-c < \bar{u}_n < 0$)

Now, $\bar{u}_n < 0$, which implies $\bar{u}_n - c < 0$. However, $\bar{u}_n + c \in (0, c)$, in particular $\bar{u}_n + c > 0$. This means that the characteristics corresponding to the eigenvalues \bar{u}_n and

$\bar{u}_n - c$ are incoming whereas the characteristics corresponding to the eigenvalue $\bar{u}_n + c$ are outgoing. Looking at the definition of Λ in (67), we see that the characteristics to be set to zero correspond to the first, second, third and fifth component of V' . Thus, the far-field BC is

$$V'_b = \begin{pmatrix} 0 \\ 0 \\ 0 \\ \sum_{k=1}^M \left[n_1 \phi_k^1 + n_2 \phi_k^2 + n_3 \phi_k^3 + \frac{\bar{\zeta}}{c} \phi_k^5 \right] a_k(t) \\ 0 \end{pmatrix} \quad (73)$$

It follows that the boundary integral component $I_{F_{jk}}$ reduces to

$$I_{F_{jk}} = \int_{\partial\Omega_F} d_4(\mathbf{x}) \left[n_1 \phi_k^1 + n_2 \phi_k^2 + n_3 \phi_k^3 + \frac{\bar{\zeta}}{c} \phi_k^5 \right] dS \quad (74)$$

3. Case 3: Subsonic Outflow ($0 < \bar{u}_n < c$)

In this case, $\bar{u}_n > 0$ implies that $\bar{u}_n + c > 0$ but $\bar{u}_n \in (0, c) \Rightarrow \bar{u}_n - c \in (-c, 0)$, i.e., $\bar{u}_n - c < 0$. This means that the characteristics corresponding to $\bar{u}_n - c$ are incoming whereas the characteristics corresponding to the other two eigenvalues are outgoing. It follows that the far-field BC to be implemented is

$$V'_b = \begin{pmatrix} \sum_{k=1}^M \left[n_1 \left(\phi_k^4 + \left(\frac{\bar{\zeta}}{c} \right)^2 \phi_k^5 \right) - n_2 \phi_k^3 + n_3 \phi_k^2 \right] a_k(t) \\ \sum_{k=1}^M \left[-n_1 \phi_k^3 - n_2 \left(\phi_k^4 + \left(\frac{\bar{\zeta}}{c} \right)^2 \phi_k^5 \right) + n_3 \phi_k^1 \right] a_k(t) \\ \sum_{k=1}^M \left[-n_1 \phi_k^2 + n_2 \phi_k^1 + n_3 \left(\phi_k^4 + \left(\frac{\bar{\zeta}}{c} \right)^2 \phi_k^5 \right) \right] a_k(t) \\ \sum_{k=1}^M \left[n_1 \phi_k^1 + n_2 \phi_k^2 + n_3 \phi_k^3 + \frac{\bar{\zeta}}{c} \phi_k^5 \right] a_k(t) \\ 0 \end{pmatrix} \quad (75)$$

and the desired boundary integral is

$$I_{F_{jk}} = \int_{\partial\Omega_F} \left\{ d_1(\mathbf{x}) \left[n_1 \left(\phi_k^4 + \left(\frac{\bar{\zeta}}{c} \right)^2 \phi_k^5 \right) - n_2 \phi_k^3 + n_3 \phi_k^2 \right] \right. \\ + d_2(\mathbf{x}) \left[-n_1 \phi_k^3 - n_2 \left(\phi_k^4 + \left(\frac{\bar{\zeta}}{c} \right)^2 \phi_k^5 \right) + n_3 \phi_k^1 \right] \\ + d_3(\mathbf{x}) \left[-n_1 \phi_k^2 + n_2 \phi_k^1 + n_3 \left(\phi_k^4 + \left(\frac{\bar{\zeta}}{c} \right)^2 \phi_k^5 \right) \right] \\ \left. + d_4(\mathbf{x}) \left[n_1 \phi_k^1 + n_2 \phi_k^2 + n_3 \phi_k^3 + \frac{\bar{\zeta}}{c} \phi_k^5 \right] \right\} dS \quad (76)$$

4. Case 4: Supersonic Outflow ($\bar{u}_n > c$)

Here, $\bar{u}_n > c \Rightarrow \bar{u}_n - c, \bar{u}_n + c > 0$, i.e., all the characteristics are outgoing. Hence the boundary integral is unaltered.